Supporting Information

Liquid Metal Eutectic Gallium–Indium (EGaIn) Blended with Paraffinic Wax for Enhanced Solar-to-Heat Conversion

Hyeonmin Jo,[†,1] Somnath Chowdhury,[†,2] Chimin Song,[†,1] Eunju Na,[1] Minjeong Cho,[1] Sung Gu Kang,[,2] Joohyung Lee[*,1]*

[1]Department of Chemical Engineering, Myongji University, 116 Myongji-ro, Cheoin-gu, Yongin-si, Gyeonggi-do, 17058, Korea

[2]School of Chemical Engineering, University of Ulsan, 93 Daehak-ro, Nam-gu, Ulsan-si, 44610, Korea

[†]These authors contributed equally to this work.

[*]**Corresponding Authors**

Sung Gu Kang (sgkang@ulsan.ac.kr), Joohyung Lee (ljbro@mju.ac.kr)

Experimental Details

Materials. EGaIn (75 wt% Ga and 25 wt% In) was obtained from Suzhou Chuanmao Metal Materials Co., Ltd. (China). $C_{20}H_{42}$ was purchased from Alfa Aesar (USA). PVA was purchased from Daejung Chemicals & Metals Co., Ltd. (Korea). Deionized water (resistivity: 18.2 MΩ·cm) was produced using the Direct-Q water purification system (Millipore, USA).

Sample Preparation. EGaIn and $C_{20}H_{42}$with various EGaIn:$C_{20}H_{42}$ volume ratios (10:0, 9:1, 8:2, 7:3, 6:4, 5:5, 4:6, 3:7, 2:8, or 1:9) were mixed using a porcelain mortar and pestle for approximately 60 min to prepare precursor mixtures. To produce EGaIn–$C_{20}H_{42}$ hybrid particles, the precursor mixtures at selected EGaIn:$C_{20}H_{42}$ volume ratios were emulsified with an aqueous PVA solution (20 wt% PVA) at precursor mixture:PVA solution volume ratios of 5:5 using the mortar and pestle for approximately 1 min. 0.3 mL of the as-prepared emulsions containing suspended EGaIn–$C_{20}H_{42}$ hybrid particles were manually coated onto glass substrates (20 mm × 20 mm; Cat. No. 1000412; Marienfeld, Germany) and left at ambient conditions for at least 24 h to allow water evaporation.

Solar-to-Heat Conversion. The glass substrates coated with hybrid particles at selected EGaIn:$C_{20}H_{42}$ ratios were subjected to simulated solar irradiation (AM 1.5G filter) at 1 SUN (1 kW/m²) intensity using a SciSun-300 solar simulator (Sciencetech, Canada) for 20 min. Afterwards, the surfaces were left at ambient conditions without irradiation for an additional 4 min. The temperature variations on the surfaces were monitored using an Optrix Xi 400 infrared camera (Optris Infrared Sensing, LLC, USA). Since the photothermal specimens were coated with a residual PVA binder (fixed at 16.7 vol.% for all samples) after water evaporation, a fixed emissivity value of 0.95 was used, consistent with the standard values typically used for polymeric, painted, oxidized, and other nonmetallic surfaces (≈0.90–0.98). To verify the

accuracy of the temperature measurements, contact thermocouples were simultaneously placed at representative positions on the surface. The temperatures recorded by the thermocouples differed from the IR readings by less than ±0.53 °C, confirming the reliability of the reported data. Each measurement was repeated at least three times to ensure the statistical reliability of the observed results.

Characterization. XRD patterns of the EGaIn, $C_{20}H_{42}$, and their precursor mixtures were obtained using an Aeries 600 (Malvern Panalytical, Netherlands). ATR-FTIR analysis of the EGaIn–$C_{20}H_{42}$ precursor mixtures and emulsified hybrid particles was performed with an IRTracer-100 (Shimadzu, Japan) spectrometer. A BX51 polarized optical microscope (Olympus, Japan) was employed to observe the morphology of EGaIn–$C_{20}H_{42}$ hybrid particles. An EM-30 SEM equipped with EDS (COXEM, Korea) was used to investigate the detailed morphology of the hybrid particles. A Discovery DSC 25 (TA Instruments, USA) was used to characterize the latent heat absorption and release behaviors of the hybrid particles in the temperature range of 25–55 °C at a scanning rate of 5 °C/min under an N_2 environment. A K-Alpha+ XPS apparatus (Thermo Fisher Scientific, USA) with an Al Kα microfocused monochromator (1486.6 eV) was used to investigate the surface chemistry of the hybrid-coated surfaces at selected EGaIn:$C_{20}H_{42}$ ratios. For depth profiling analysis, Ar ion beam etching (1 keV) was conducted. Reflectance of hybrid particle-coated surfaces over 250–2500 nm was measured using a Lambda 750 spectrophotometer (PerkinElmer, USA), with values reported relative to a white reference (100%).

Computational Details. Density functional theory (DFT) was utilized for calculations within the Vienna Ab initio Simulation Package (VASP; *Phys. Rev. B* **1996**, *54*, 11169; *Comput. Mater. Sci.* **1996**, *6*, 15). The projector-augmented wave (PAW; *Phys. Rev. B* **2005**, *71*, 035109)[41] was

used. We used a plane-wave cut-off energy of 400 eV. The generalized gradient approximation (GGA), based on the Perdew–Burke–Ernzerhof (PBE) functional (*Phys. Rev. Lett.* **1996**, *77*, 3865), was utilized as the foundation for the exchange-correlation functional. A 50 Å vacuum region was added in the z-direction. To optimize geometry, Monkhorst–Pack (*Phys. Rev. B* **1976**, *13*, 5188) *k-points* of (3 × 3 × 1) were used. The energy convergence criteria were set at 10^{-6} eV throughout the self-consistent field iteration. Atomic geometries were optimized until all atoms' forces converged to less than 0.01 eV/Å. The DFT-D3 was implemented to consider the van der Waals (vdW) interactions (*J. Phys. Chem. C* **2014**, *118*, 7615). For the computational modeling of EGaIn bulk alloy, we employed a stoichiometric ratio of Ga:In = 3:1. Hexagonal and cubic bulk structures were first studied (**Figure S5a**), revealing the hexagonal structure to be energetically favored. The (100), (110), and (111) surfaces were then cleaved from the hexagonal bulk and optimized, identifying the (100) surface as the most stable facet (**Figure S5b**). PDOS calculation for the pristine (100) surface was performed to determine the Fermi level (E_f) (**Figure S5c**). Similarly, bulk β-Ga_2O_3 and its cleaved (100), (110), and (111) surfaces were analyzed, with the (100) surface being most stable (**Figure S6a**). The EGaIn–Ga_2O_3 heterostructure was constructed using a [2×6×1] supercell of (100) EGaIn and a [4×5×1] supercell of (100) Ga_2O_3 (Figure S6b), and its PDOS and E_f were calculated (Figure S6c). Finally, the EGaIn–$C_{20}H_{42}$ heterostructure was modeled using a [6×3×1] supercell of the (100) EGaIn surface and the optimized paraffin structure, with PDOS calculations performed and the E_f determined.

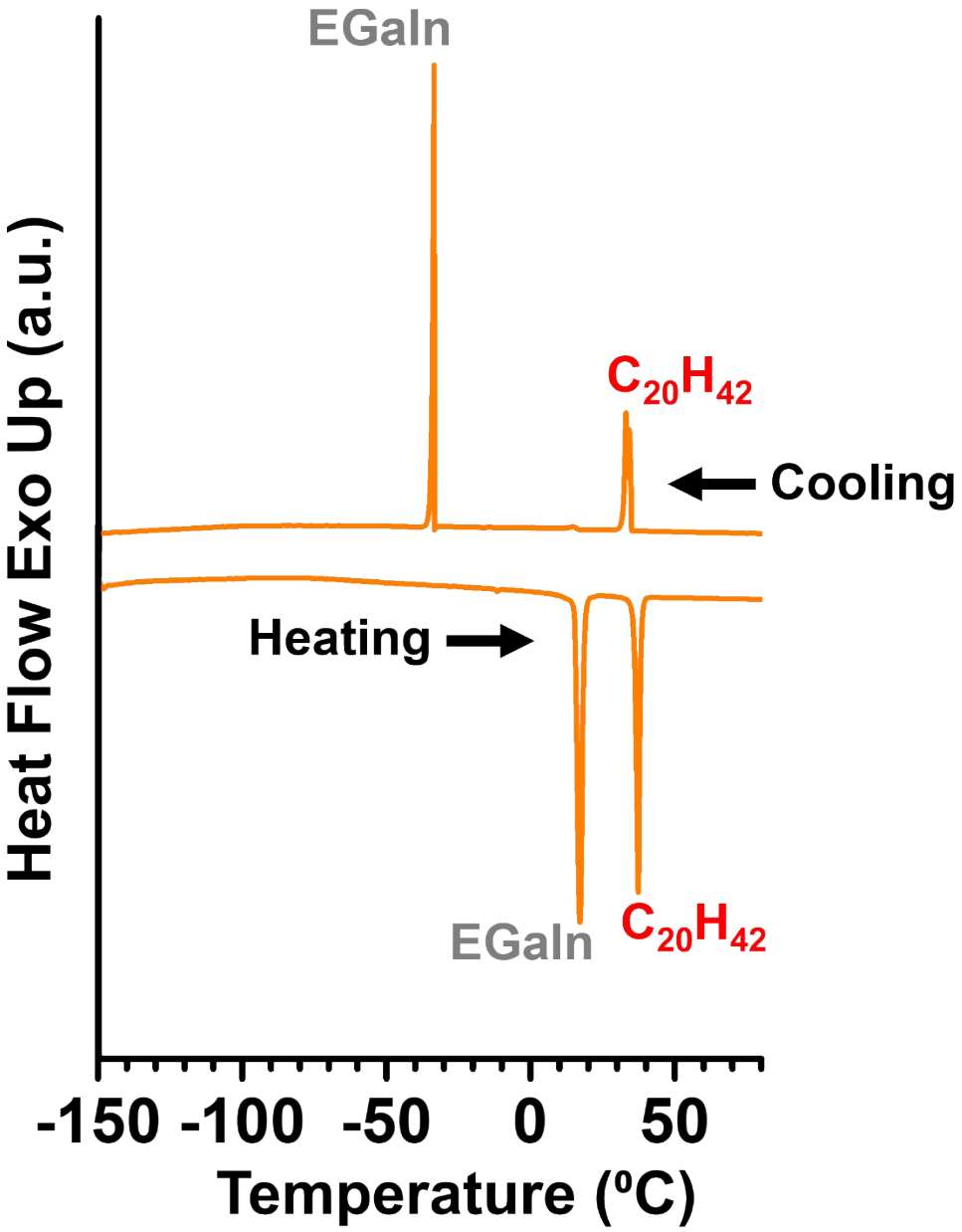

Figure S1. DSC heating and cooling curves of an EGaIn–$C_{20}H_{42}$ precursor mixture with EGaIn:$C_{20}H_{42}$ volume ratios of 3:7. During heating, substantial endothermic peaks were observed at 16.8 °C and 37 °C, which correspond to the melting of EGaIn and $C_{20}H_{42}$, respectively. During cooling, an exothermic peak first appeared at 35.3 °C, attributed to the crystallization of $C_{20}H_{42}$. Upon further cooling, another exothermic peak emerged at −33.8 °C, originating from the crystallization of EGaIn. The significant suppression of the freezing point relative to the melting point is attributed to the supercooling behavior of EGaIn (*Adv. Func. Mater.* **2019**, *29*, 1906098).

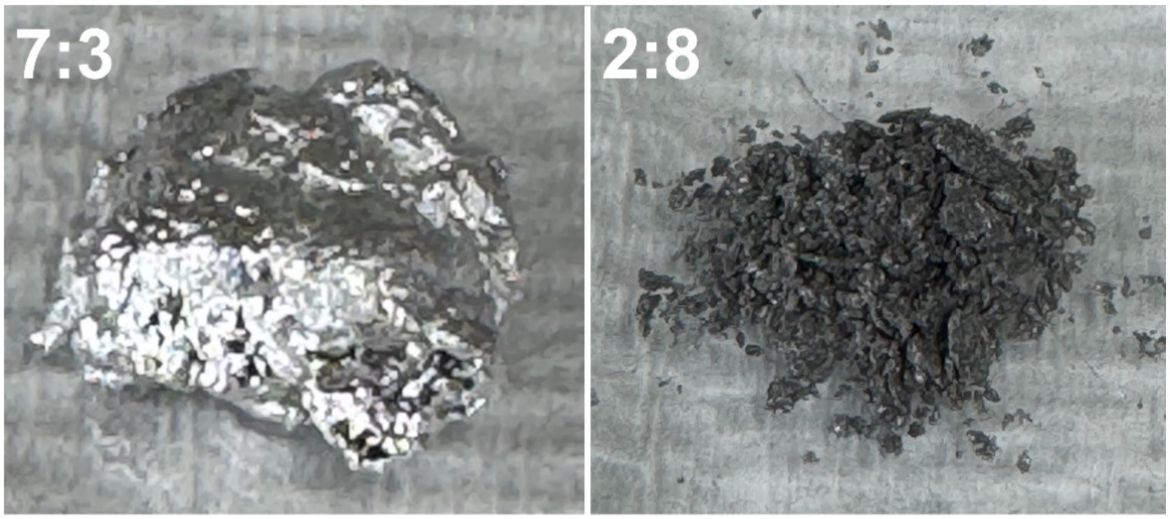

Figure S2. Photographs of EGaIn–rich (7:3) and $C_{20}H_{42}$-rich (2:8) precursor mixtures after storage for > 1 year under ambient conditions.

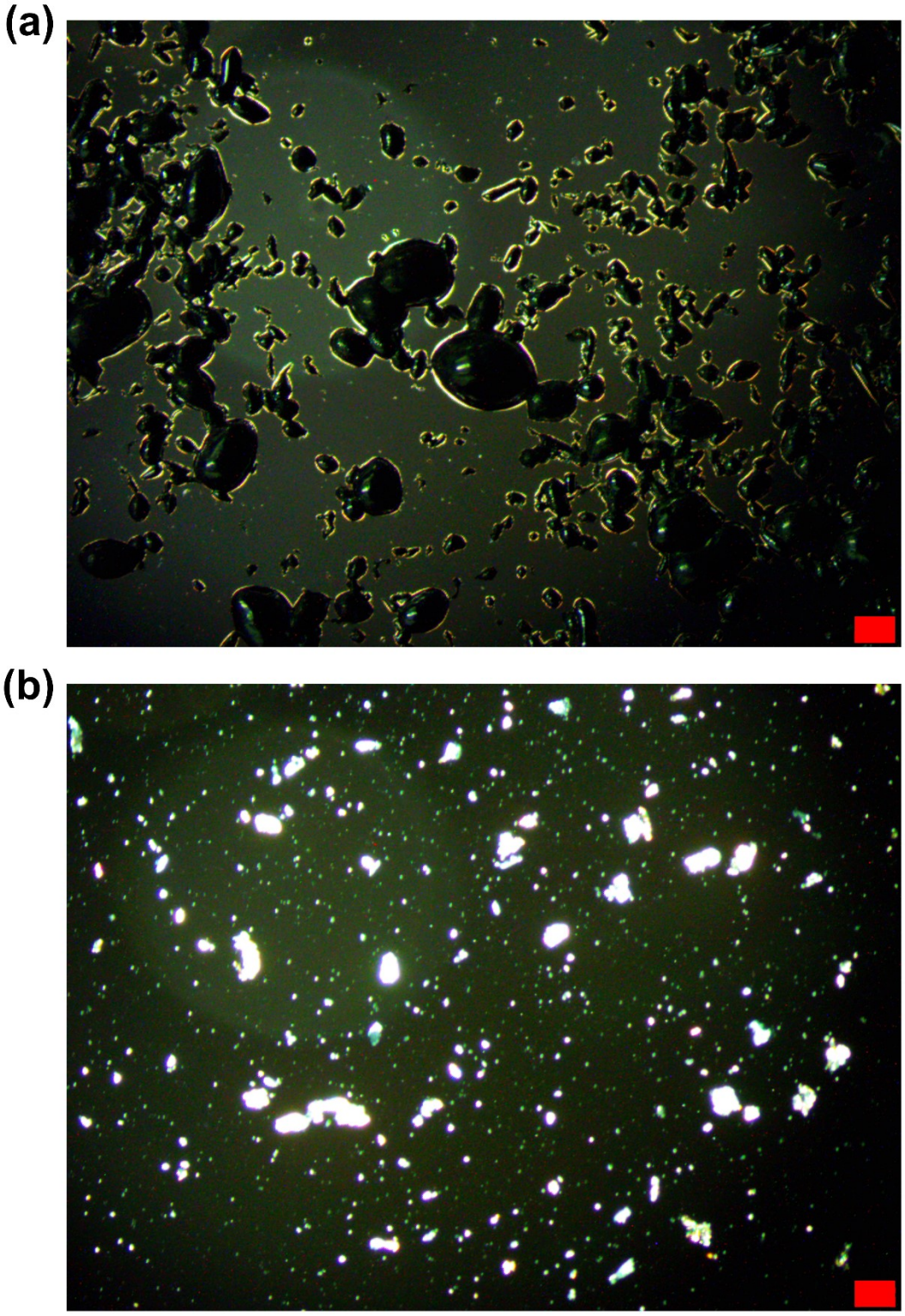

Figure S3. Polarized light microscopy images of (a) EGaIn (10:0) and (b) $C_{20}H_{42}$ (0:10) particles (scale bars: 100 μm).

(a)

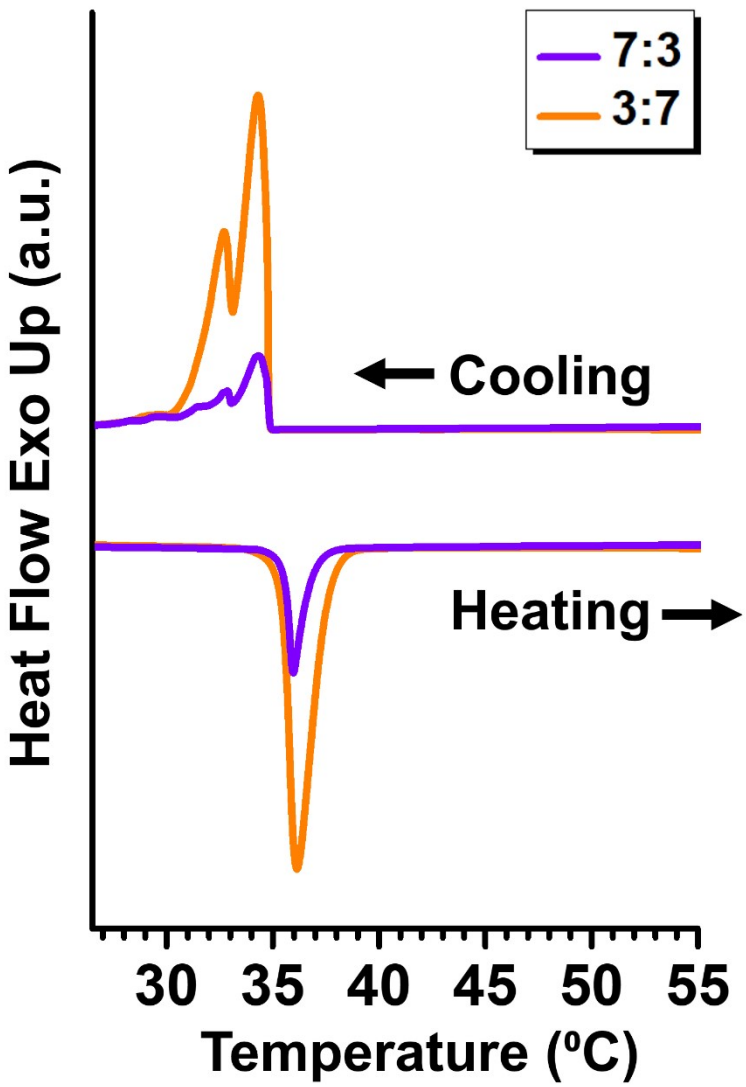

(b)

EGaIn:$C_{20}H_{42}$	ΔH_m (in J/g)	ΔH_c (in J/g)	ΔH_t (in J/g)
7:3	10.25	10.45	10.38
3:7	43.41	43.30	44.45

Figure S4. (a) DSC heating and cooling curves of the EGaIn–$C_{20}H_{42}$ hybrid particles at selected EGaIn:$C_{20}H_{42}$ volume ratios, prepared using a different $C_{20}H_{42}$ product. (b) Experimental melting (ΔH_m) and crystallization (ΔH_c) enthalpies, and theoretical enthalpy (ΔH_t). The ΔH_t values were estimated by multiplying the mass fraction of $C_{20}H_{42}$ in each hybrid formulation by the enthalpy of 213.8 J/g for the new $C_{20}H_{42}$ bulk product.

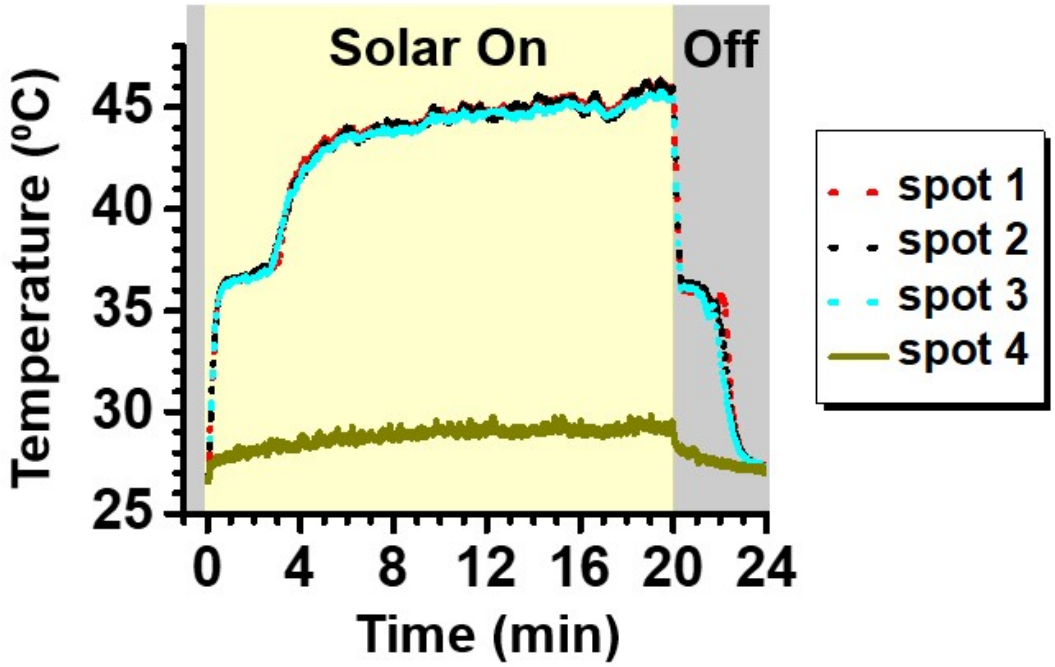

Figure S5. Temperatures at three points (spot 1, 2, and 3) on a hybrid-coated surface and one point (spot 4) outside the coated surface, represented as functions of time (solar on: 0–20 min; solar off: 20–24 min). The hybrid used had an EGaIn:$C_{20}H_{42}$ volume ratio of 2:8.

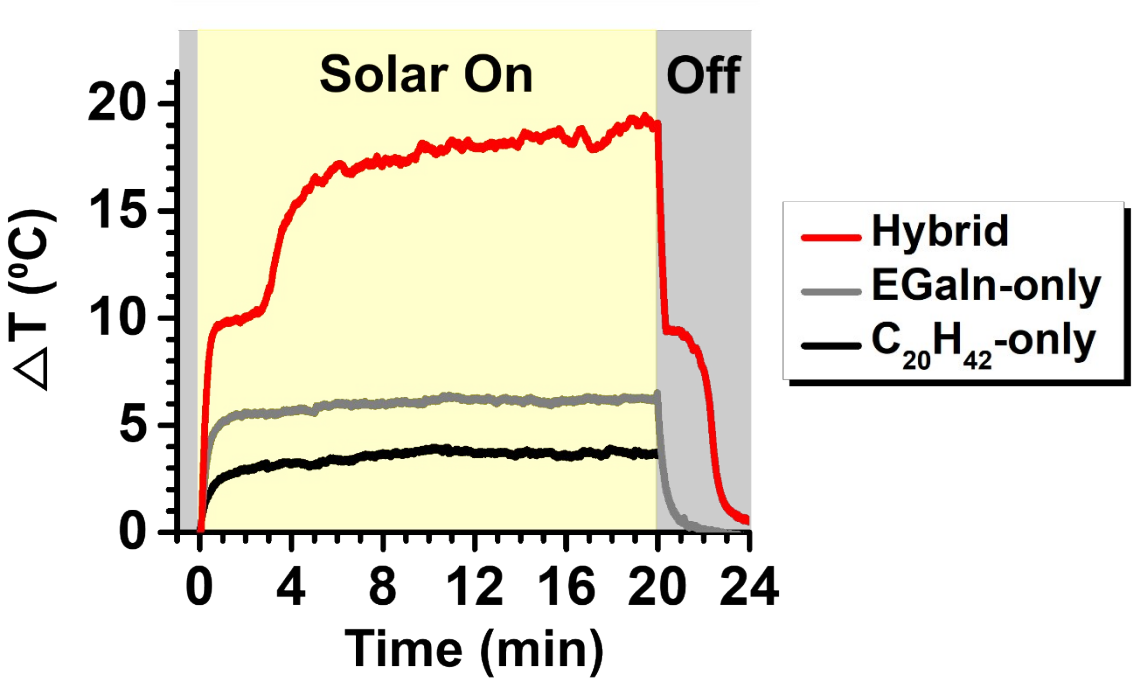

Figure S6. Temperature variations (ΔT) on surfaces coated with $C_{20}H_{42}$-only (0:10), EGaIn-only (10:0), and hybrid (2:8) particles, represented as functions of time (solar on: 0–20 min; solar off: 20–24 min).

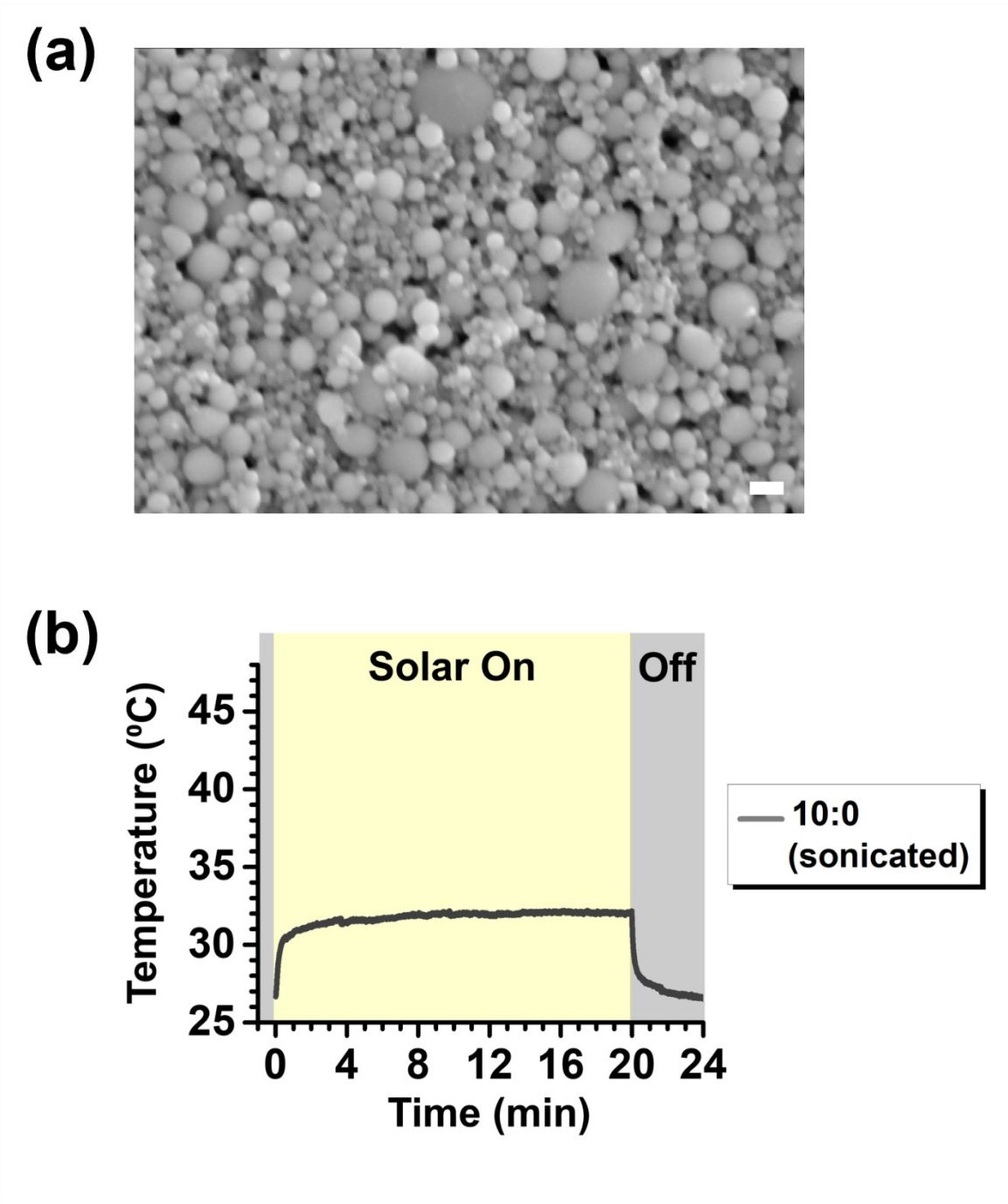

Figure S7. (a) SEM image of ultrasonicated EGaIn particles (10:0) (scale bar: 1 μm). (b) Average temperature of three points on the ultrasonicated EGaIn particle (10:0)-coated surface, represented as a function of time (solar on: 0–20 min; solar off: 20–24 min).

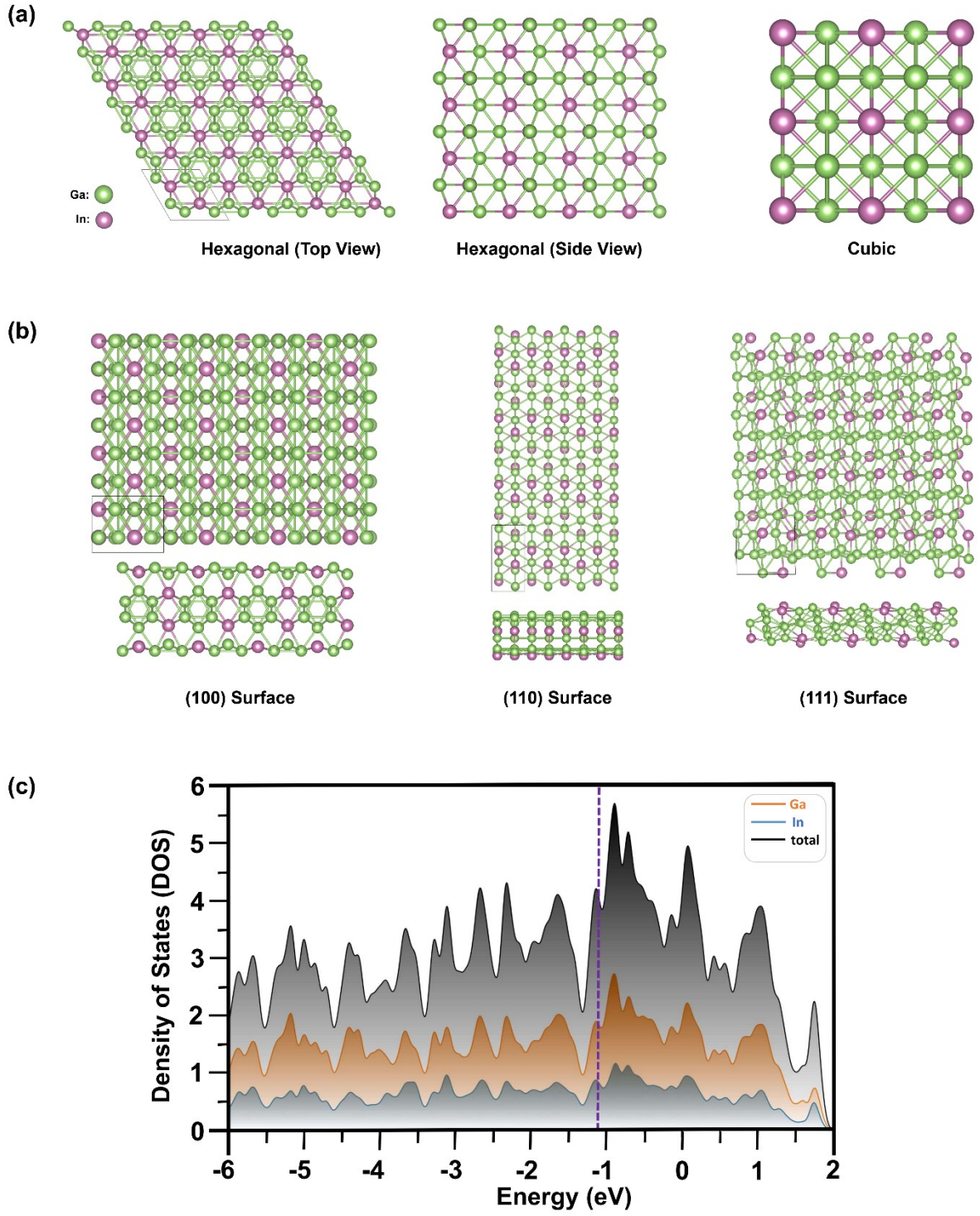

Figure S8. DFT optimized geometries of (a) hexagonal (top and side view) and cubic bulk structures of EGaIn. (b) (100), (110), and (111) surfaces of the hexagonal EGaIn bulk. (c) Density of states of the pristine (100) surface of EGaIn, with the dotted vertical line (purple color) indicating the Fermi energy level (E_f = –1.14 eV).

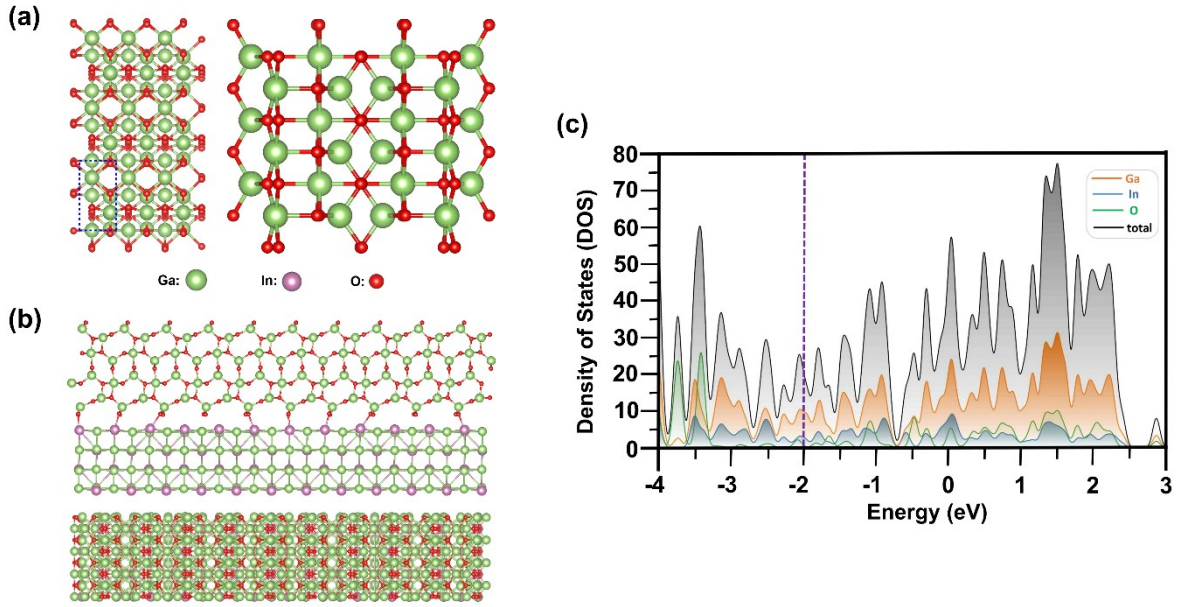

Figure S9. DFT optimized geometries of (a) (100) β-Ga_2O_3 surface and (b) the EGaIn–Ga_2O_3 composite. (c) Density of states of the EGaIn–Ga_2O_3 composite, with the dotted vertical line (purple color) indicating the Fermi energy level (E_f = –2.01 eV).

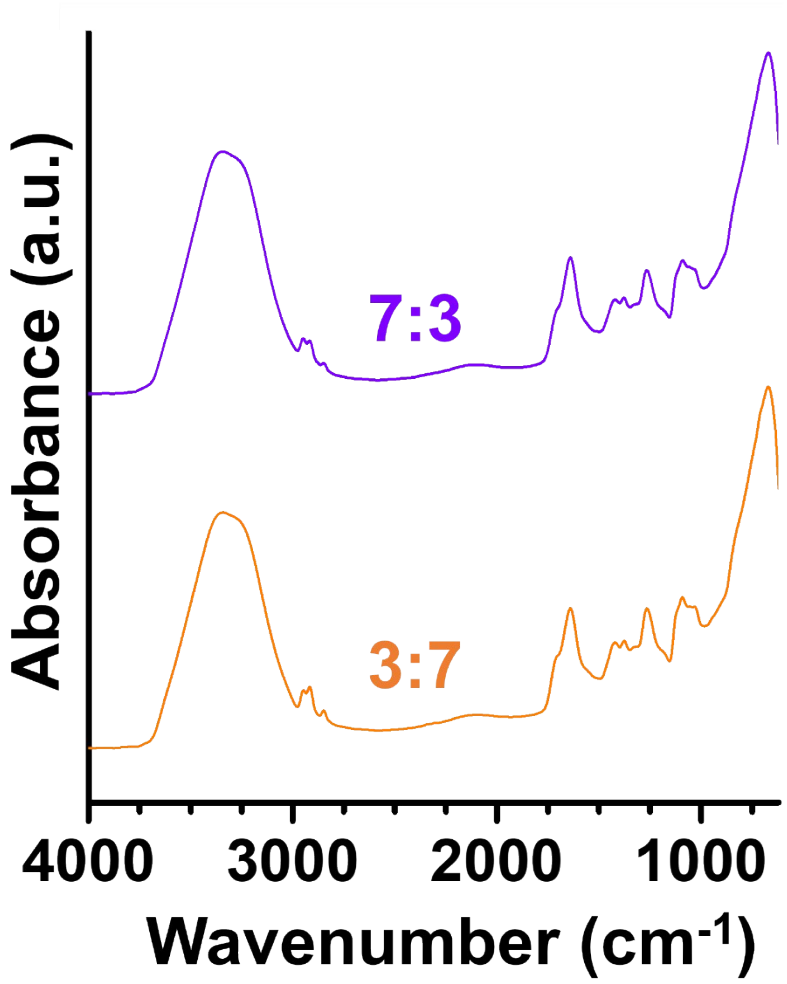

Figure S10. ATR-FTIR spectra of EGaIn-rich (7:3) and $C_{20}H_{42}$-rich (3:7) hybrid particles, obtained from PVA-mediated emulsions after water evaporation. The bands at 3338 cm^{-1} and 1639 cm^{-1} can be attributed to O–H stretching and bending vibrations, respectively, which may originate from the hydroxyl groups of PVA and adsorbed water. The peak at 1720 cm^{-1} corresponds to C=O stretching derived from residual acetyl groups in PVA, while the absorptions at 1267 cm^{-1} and 1091 cm^{-1} are assigned to C–O stretching of PVA. The peaks at 2949, 2918, 2848, 1421, and 1377 cm^{-1} are associated with CH_2 and CH_3 groups commonly present in both $C_{20}H_{42}$ and PVA. The broad band around 671 cm^{-1} is likely due to the overlapping contributions of Ga–O vibrations from the surface oxide layer formed on EGaIn droplets and C–H vibrations from $C_{20}H_{42}$ and PVA. The FTIR spectra of both EGaIn-rich and $C_{20}H_{42}$ -rich hybrids are dominated by PVA adsorbed on the surfaces of the hybrid particles, and no significant structural shifts in the peaks were observed with increasing $C_{20}H_{42}$ content. At the very least, this comparison supports that the formation of new bulk compounds is minimal, even when the $C_{20}H_{42}$ fraction is increased, which had previously led to a pronounced enhancement in photothermal conversion.

Work of Adhesion

To determine the work of adhesion between the native oxide surface of EGaIn and the paraffinic $C_{20}H_{42}$ surface, the Owens–Wendt–Rabel–Kaelble (OWRK) method, based on Fowkes' classical surface thermodynamic theory (*Ind. Eng. Chem.* **1964**, *56, 40*; *J. Appl. Polym. Sci.* **1969**, *13*, 1741), was employed. In this theory, the surface energy (γ_i, in mJ/m^2) of a species *i* is expressed as the sum of its dispersive (γ_i^D) and polar (γ_i^P) components:

$$\gamma_i = \gamma_i^D + \gamma_i^P.$$

The values of γ_i^D and γ_i^P for a given material can be estimated by measuring the contact angles of several probe liquids with known γ_i^D and γ_i^P on the target surface. The total work of adhesion (W_{1-2}) between two surfaces (1 and 2) is likewise the sum of the dispersive and polar contributions:

$$W_{1-2} = W_{1-2}^{D} + W_{1-2}^{P}$$

where

$$W_{1-2}^{D} = -2\sqrt{\gamma_1^D \gamma_2^D} \text{ and } W_{1-2}^{P} = -2\sqrt{\gamma_1^P \gamma_2^P}.$$

Under ambient conditions, the EGaIn surface is naturally covered by a native oxide layer. The dispersive (γ_{oxide}^{D}) and polar (γ_{oxide}^{P}) components for this surface were taken from our previous measurements (*Adv. Mater. Interfaces* **2023**, *10,* 2202527). For the paraffinic $C_{20}H_{42}$ surface, the polar contribution is practically negligible ($\gamma_{paraffin}^{P} \approx 0$) owing to its nonpolar nature. Therefore, the total surface tension ($\gamma_{paraffin}$) measured for molten $C_{20}H_{42}$ at 313.15 K (*J.*

Chem. Eng. Data **2002**, *47,* 1442) was used to estimate $\gamma_{paraffin}^{D}$. The obtained parameters are summarized in **Table S1**, from which $W_{oxide-oxide}$ and $W_{oxide-paraffin}$ were estimated.

Table S1. Surface energy components of the interacting species.

Material	**Surface Energy Component (in mJ/m^2)**	
	γ_i^D	γ_i^P
EGaIn (native oxide)	49.8	16.4
$C_{20}H_{42}$ (paraffin)	27.6	≈ 0

Photothermal Conversion Efficiency

The steady-state photothermal conversion efficiencies (η) of EGaIn–$C_{20}H_{42}$ hybrids with various EGaIn:$C_{20}H_{42}$ ratios were calculated from the balance between absorbed solar energy and the total heat dissipated to the environment:

$$\eta = \frac{h\,S\,(T_{max} - T_{surr})}{q\,A} \tag{1}$$

where h denotes the heat-transfer coefficient, S is the surface area contributing to heat loss, T_{max} is the maximum temperature in the steady-state regime under illumination, T_{surr} is the ambient temperature, q is the solar flux (1 kW/m², equivalent to 1 SUN), and A represents the irradiated area (*ACS Nano* **2022**, *16*, 15086; *Small* **2022**, *18*, 2104048; *Chem. Eng. J.* **2024**, *489*, 151338). Here, the h value was derived from the post-irradiation cooling profile, $T(t)$ *versus* t (where $T(t)$ is the transient specimen temperature and t is time), for the $C_{20}H_{42}$–free EGaIn system (10:0) to avoid the underestimation of h caused by the latent-heat release from the $C_{20}H_{42}$-loaded hybrid systems. By applying a lumped-parameter model, the relative temperature $\theta(t)$ is defined as

$$\theta(t) = \frac{T(t) - T_{\text{surr}}}{T_{max} - T_{\text{surr}}} = exp(-\frac{t}{\tau}) \tag{2}$$

where the characteristic time constant τ is given by

$$\tau = \frac{\sum_i m_i c_{p,i}}{h\,S} \tag{3}$$

with m_i and $c_{p,i}$ representing the mass and specific heat capacity of each composite component, respectively. The obtained h value was substituted into Eq. (1) to compute η values for the hybrid systems with various EGaIn:$C_{20}H_{42}$ ratios.

Table S2. Summary of engineered LM systems and their maximum temperatures (T_{max}) achieved under 1 SUN solar irradiation in ambient conditions, along with photothermal conversion efficiencies (η).

System Description	T_{max} (°C)	η (%)	Reference
EGaIn functionalized with stearic acid through the formation of $(2C_{17}H_{35}COO)_3Ga$ bonds	56.7	N/A	*Nano Energy* **2021**, *86*, 106138
Ga "layer" completely painted with a tannic acid-Fe^{3+}-Ti^{4+} coordination complex ink	56.2	93	*Adv. Mater.* **2024**, *36*, 2308346
EGaIn coupled with polydopamine-reduced graphene oxide multilayers	52.5	89.4	*ACS Nano* **2022**, *16*, 15086
EGaIn simply blended with paraffin wax	**45.7**	**83.3**	**This Study**
EGaIn functionalized with a gallic acid assembly-Fe^{3+} complex	45.1	83.1–89.7	*Small* **2023**, *19*, 2302526
EGaIn functionalized with polyphenol	42.3	77.3	*Small* **2022**, *18*, 2104048
EGaIn functionalized with allyl glycidyl ether-grafted tannic acid	42.3	67.5	*ACS Nano* **2024**, *18*, 5847